9

Freezing Properties of Disaccharide Solutions: Inhibition of Hexagonal Ice Crystal Growth and Formation of Cubic Ice

Tsutomu Uchida[1], Satoshi Takeya[2],
Masafumi Nagayama[1] and Kazutoshi Gohara[1]
[1]*Faculty of Engineering, Hokkaido University,*
[2]*Research Institute of Instrumentation Frontiers,*
National Institute of Advanced Industrial Science and Technology (AIST),
Japan

1. Introduction

Numerous studies have been undertaken to preserve living bodies and cells from freezing by addition of cryoprotective agents including natural substances (e.g., sugars and proteins) and synthetic chemicals (e.g., glycerol and dimethyl sulfoxide). Trehalose and sucrose, which consist of fructose and glucose rings connected by a glycosidic bond, are naturally occurring disaccharide compounds found in cryoprotectants. Trehalose is primarily found in animals capable of enduring cold temperatures, whereas sucrose is typically found in plants (Crowe et al., 1988). Since these molecules are too large to permeate the biomembrane, the cryoprotective mechanism is considered to be different from those of cell-permeable substances, such as glycerol and dimethyl sulfoxide.

One of the considerable mechanisms of disaccharide molecules operating as a cryoprotective agent of living cells is that they protect the lipid bilayer by making the hydrogen bonding during extracellular ice formation. Based on the interactions between disaccharide molecules and the lipid bilayer, it has been suggested that the molecular mechanism underlying this cryoprotective effect is the hydrogen bonding of trehalose molecules to the bilayer head group (Sum et al., 2003). A simulation of the interaction of the lipid bilayer with trehalose has revealed that only marginal changes occur in the lipid bilayer.

Another considerable mechanism of disaccharide molecules of the cryoprotective effect for living cells is that they inhibit the growth of ice crystals in extracellular space. To reveal the inhibition mechanism of disaccharides on ice crystal growth, the interaction between the disaccharide and water molecules has been investigated both by macroscopic observations (for example, Sei et al., 2001; 2002; Sei & Gonda, 2004), where the melting point of disaccharide solutions has been determined, and by microscopic observations (for example, Wang & Tominaga, 1994; Kanno & Yamazaki, 2001; Akao et al., 2001; Branca et al., 1999a) where the interaction has been investigated via Raman or infra-red spectroscopy. Sei et al. (2001; 2002) found that the melting points of trehalose and sucrose solutions were lower than those expected by the molar freezing point depression. They explained this phenomenon by considering the ratio of the hydrated water around disaccharide molecules

to that of free water, because these disaccharides interact with water strongly. Therefore, the cryoprotective mechanism of disaccharide is considered to be controlled by the hydration of disaccharide molecules in solution. Raman spectroscopic observations have revealed that disaccharides promote a destructive effect on the tetrahedral hydrogen-bond network of pure water (Branca et al., 1999a). The results of such studies have led to the hypothesis that disaccharides obstruct the crystallization process, thereby destroying the network of water in a manner similar to that occurring in ice. This hypothesis qualitatively coincides with the conclusions suggested by the ice single-crystal observations (Sei et al., 2002). However, the cyroprotective mechanisms of the living cells by these cell-impermeable protectants are still under consideration.

Based on the application of disaccharides to the sample preparation for the electron microscopic observation, it is believed that the quenching process allows forming amorphous phase, which inhibits the ice crystal growth and thus protects from damage the living cells or objective samples during freezing. However, the observations of molecular conditions in solution are very difficult due to the limitations of temporal and spatial resolutions. Uchida and coworkers have investigated the effects of cryoprotectant materials on the inhibition mechanism of ice growth. By using the freeze-fracture replica technique and a field-emission gun type transmission electron microscope (FEG-TEM), they investigated the nano-scale size molecular conditions in the disaccharide solutions (Uchida et al., 2007). To determine the materials observed in the replica images, they carried out the x-ray diffraction experiments on the similarly prepared disaccharide solution samples (Uchida & Takeya, 2010). They identified each phase observed in the TEM images, and they revealed the frozen state of both disaccharide molecules and water molecules. In addition, they discovered the formation of metastable phase of ice, ice Ic, and its anomalous stability at higher temperature conditions. In section 2, these morphological investigations of the quenched disaccharide solutions are reviewed. In order to investigate the structuring of solution prior to the freezing, which affects the growth process of ice crystal, the temperature and concentration dependences of viscosity of disaccharide solutions were required to be measured. Uchida et al. (2009) measured the viscosity of trehalose solutions by a dynamic light-scattering (DLS) spectroscopy (section 3). Since these investigations allowed us to discuss the inhibition process of disaccharide molecules for the ice crystal growth in the extracellular space, we discuss the role of disaccharide molecules serving as the cryoprotectant of living cells in the final section.

2. Microscopic observation of frozen disaccharide solutions

Uchida et al. (2007) aimed to observe the solute-solution interaction in the liquid phase using a FEG-TEM along with the freeze-fractured replica technique. This technique has usually been applied for biological investigations. They performed to show it to be very useful for investigating the microstructures and the dynamic features of solutes in the solution when a small droplet is quenched at liquid nitrogen temperature. However, the replica cannot determine the substances observed in TEM image. Thus they carried out the powder x-ray diffraction (PXRD) measurements for samples prepared under similar conditions (Uchida & Takeya, 2010).

They focused primarily on trehalose, which has been considered as one of the cryoprotective agents that reduces the freezing rate of ice (Sei & Gonda, 2004). Research-grade trehalose

dihydrate crystals were donated by Hayashibara Biochemical Laboratories, Inc. To compare the properties observed in the various trehalose solutions, they conducted similar investigations using sucrose (of the highest quality; Sigma-Aldrich Japan, Inc.) and maltose (research grade, Hayashibara Biochemical Laboratories, Inc.). The purity of the distilled and deionized water used for the solutions was confirmed by the conductivity of approximately 5×10^{-6} S m^{-1}.

They prepared the trehalose solutions which mass concentrations are ranged from 3 wt% to 50 wt%. The concentration of the solutions was determined by measuring the masses of the disaccharides and pure water taking into consideration the hydrated water of crystallization. The accuracy of the concentration measurements was estimated ±0.1 wt% at room temperature. Then, these solutions (approximately 20 mm^3) were rapidly frozen in a liquid nitrogen atmosphere (approximately 80 K). To avoid the bubbling of the solution, the sample was kept just above the liquid nitrogen surface. Under these conditions, the freezing rate was approximately 3×10^2 K min^{-1}. The order of this value was almost similar (ranging within ±50 K min^{-1}) in all trehalose solutions, even though the solutions had a relatively wide concentration range. Then, the frozen sample was introduced into the freeze-fracture replica sample preparation system (JEOL, type JFD-9010). The sample was fractured under a vacuum (10^{-5} Torr) and at a low temperature (150–170 K). A replica film of this fractured surface was prepared by evaporating platinum and carbon on it. To observe the replica samples, we used FEG-TEM (JEOL, type JEM-2010) at an accelerating voltage of 200 kV. An imaging plate was used to record the observed images.

Figures 1a–1f show the TEM images of the freeze-fractured replica samples of trehalose solutions at various concentrations. These pictures showed three typical textures: (**S**) smooth surface, (**P**) fine particles (average diameter was 20-30 nm), and (**R**) remaining part of the boundary between the smooth-surface area adjacent to the fine particles (see Figure 1d). The area of **S** at lower concentrations was so large that their precise shapes and sizes could not be determined (see Figures 1a and b) from TEM images only. However, **S** area became sufficiently small at higher trehalose concentrations. As shown in Figures1c–1f, the **S** area appeared to have oval elongated shapes in a certain direction. Further increases in the trehalose concentration led to a reduction in the size of **S** area and exhibited the crystal facets. The intermediate space consisting of **P** area also becomes large simultaneously, thus the distance between each **S** area increased.

These phenomena indicated that the **S** area was considered to be the ice crystal, and the **P** area relates to the trehalose molecules. The decrease in size and the change in morphology of **S** area would be explained by both a reduction in the amount of H_2O molecules available to form ice crystals and a decrease in the growth rate of the ice crystals. The increase in the trehalose concentration may also affect the degree of supercooling of the solution, which would control the heat conduction formed in the ice crystal. Therefore, the growth rate was controlled either by the rate of supply of H_2O molecules from the surrounding solution to the ice surface or by the heat conduction from the reaction sites. If trehalose inhibited the ice crystal growth kinetically, we would find fine particles on the edge of a smooth area. However, the TEM images reveal that only a small amount of fine particles was located just along the boundary of the **S** area. Therefore, it appears that the main rate-controlling process is the rate of supply of H_2O molecules from the solution or the rate of the latent heat conduction.

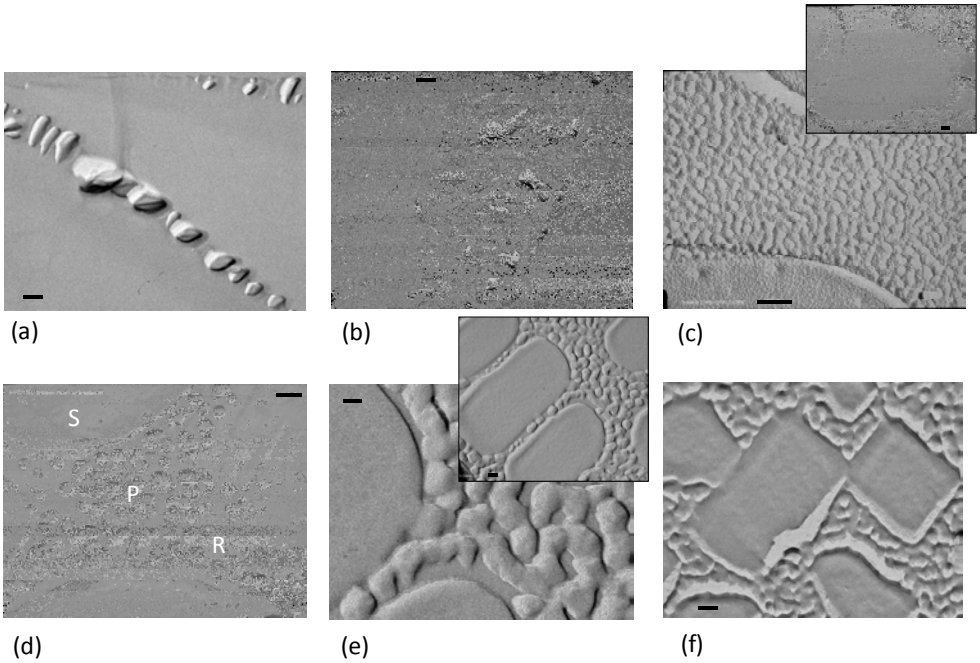

Fig. 1. (a) TEM image of an ice surface formed from trehalose solution (8.5 wt%). Scale bar: 100 nm. (b) from trehalose solution (15 wt%). Scale bar: 100 nm. (c) from trehalose solution (25 wt%). Scale bar: 100 nm. The inset was taken at a smaller magnification (scale bar: 500 nm). (d) from trehalose solution (35 wt%). Scale bar: 100 nm. (e) from trehalose solution (40 wt%). Scale bar: 100 nm. The inset picture was taken at a smaller magnification (scale bar: 200 nm). (f) from trehalose solution (50 wt%). Scale bar: 100 nm. (Reprinted from Uchida et al., 2007, with permission from Elsevier with slight arrangement.)

Figure 2 shows the distribution of ice crystals (**S** area) in terms of (a) size and (b) number concentration, depending on the trehalose concentration in the original solution. These results indicate that the size of each ice crystal is too large to be measured by TEM imaging at concentrations below 20 wt%, and very few ice crystals are present for TEM measurement. On the other hand, the size of the crystals is too small to be observed by an optical microscope at concentrations above 20 wt%. Then, TEM images revealed that the crystal size decreases exponentially to submicron orders of magnitude at 50 wt%, whereas the number density increases exponentially. Therefore, it appears that the growth rate of the ice crystals in the high-concentration trehalose solution is reduced either by a reduction in the phase-separation rate between free water and the condensed solution or by a large supply of nucleation sites for ice crystals.

Figure 3a and b show the variations in the average diameter (d_p) and the number density (N_p) of the fine particles (**P**), respectively, with respect to the trehalose concentration in the

original solution. Figure 3a shows that the d_p value of each sample exhibited weak dependence on the trehalose concentration although there were several variations in terms of the size distributions. However, N_p values were found to increase exponentially with an increase in the trehalose concentration (see Figure 3b). Note here that the gradual saturation of N_p with larger trehalose concentrations is considered to primarily result from the existence of ice crystallites in the observed area. This is supported by the fact that N_p measured in the very rapid freezing method (open square) where no ice crystallites were observed is one order of magnitude larger than that measured in the quenched sample (solid circle) at the similar trehalose concentration (approximately 35 wt%). Therefore, it was observed that **P** was almost the same size and distributed in the intermediate space of **S** area. The area occupied by particles increased with the original trehalose concentration as follows from an increase in N_p, whereas the growth of ice crystals is inhibited. The total volume of fine particles (estimated as $N_p \times \pi d_p^3/6$) increases with the trehalose concentration. These results support the assumption that the object **P** was related to trehalose molecules.

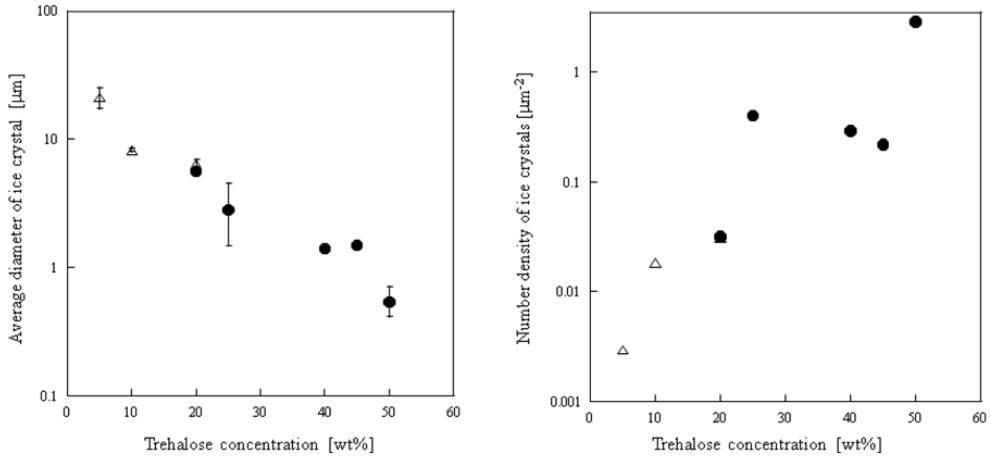

Fig. 2. (a) Dependence of the average diameter of ice crystals on trehalose concentration. Solid circles were observed via TEM and open triangles were via a polarized optical microscope (POM). (b) Dependence the number density of ice crystals on trehalose concentration. Solid circles were observed via TEM and open triangles were observed via POM. (Reprinted from Uchida et al., 2007, with permission from Elsevier.)

To determine each phase observed in the replica image, Uchida & Takeya (2010) carried out the PXRD method for the sample prepared similarity with the replica experiments. These frozen samples were finely powdered in a nitrogen atmosphere at a temperature below 100 K. The fine-powdered samples were top-loaded on a specimen holder made of Cu and mounted onto the powder x-ray diffractometer (Rigaku, type Ultima III). The PXRD measurements were done at 93 K in the $\theta/2\theta$ step scan mode with at a step 0.02 degree in the 2θ range from 6^o to 43^o using the CuKα radiation (40 kV, 40 mA).

The PXRD profiles for various concentrations of frozen trehalose solutions were shown in Figure 4. In the 23 wt% trehalose sample, typical diffraction pattern for hexagonal ice Ih (space group P_63/mmc) was observed. However, as the concentration of trehalose increased, background intensity in the 2θ range from 22° to 27° increased, which makes the line shapes broadening, and the intensity in these three peaks relatively decreased. Therefore it is considered that **S** area corresponds to the ice Ih crystallite. In addition, the relative peak intensity ratios of the ice Ih(110) and ice Ih(002) reflections changed since ice Ih(002) reflection overlaps with those of cubic ice Ic(111). These results suggest that the sample included some amount of ice Ic (space group $Fd3m$, Kuhs et al., 1987) in high concentration samples, and the volume ratio of ice Ic to Ih increased as the concentration of trehalose increased. This is the first evidence of ice Ic existence in the frozen sample of the disaccharide solutions. The ice Ic phase was observed in all the disaccharide solutions including both the sucrose and maltose solutions, especially at higher concentrations as well as in trehalose.

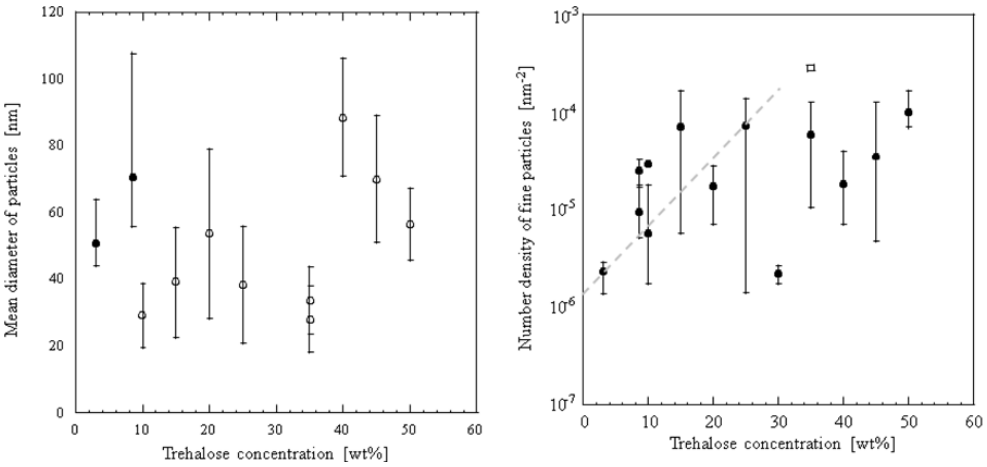

Fig. 3. (a) The average diameter of fine particles (d_p) on trehalose concentration. Open circles are estimated by fitting the log-normal distribution functions. The error bars show the standard deviations obtained by the curve fitting of each log-normal distribution. Solid circles are estimated by the arithmetic mean value because of the limited number of particles. The error bars for them denote the minimum and maximum diameter observed in the same sample. (b) The number density of fine particles (N_p) dependence on trehalose concentration. The open square denotes the average number density of the fine particles observed in the very rapid freezing method. The error bar shows the maximum variations of the measured N_p values in the same sample. Dashed line shows that N_p increases exponentially with the trehalose concentration. The gradual deviation from the dashed line at higher concentrations would be caused by the existence of ice crystallites in TEM images. (Reprinted from Uchida et al., 2007, with permission from Elsevier with slight arrangement.)

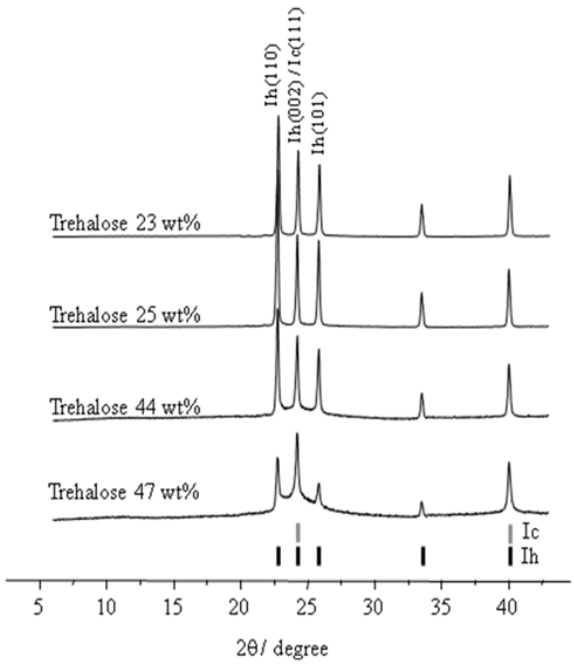

Fig. 4. PXRD patterns of rapidly frozen samples of various concentrations of trehalose solutions. The short bars indicate the positions of the diffraction patterns for both hexagonal ice Ih and cubic ice Ic. (Uchida & Takeya, 2010; reproduced by permission of the PCCP Owner Societies)

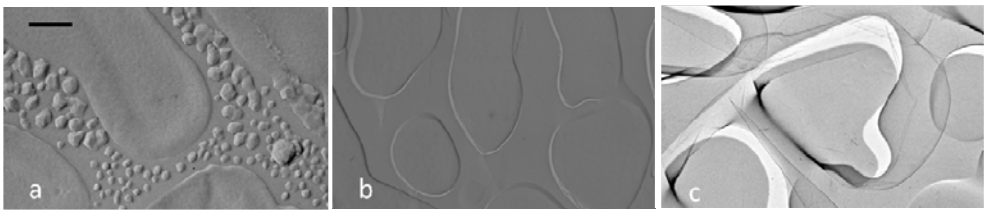

Fig. 5. TEM images of the ice surface formed from trehalose solution (35 wt%) fractured at temperatures (a) approximately 90 K, (b) approximately 180 K, and (c) approximately 250 K. Scale bar: 500 nm. (Reprinted from Uchida et al., 2007, with permission from Elsevier with slight arrangement.)

Uchida et al. (2007) investigated the temperature variation of **S** and **P** area distributions with the extent of sample annealing at higher temperatures. They prepared three frozen samples from the same 35 wt% trehalose solution. Then, sample (a) was fractured at a temperature of approximately 90 K to obtain the reference sample. Sample (b) was stored in a vacuum chamber and heated at a temperature of approximately 180 K. After approximately one hour the sample was fractured to form the replica. Sample (c) was heated to approximately 250 K,

which is sufficiently higher than the vitrification temperature (T_g') of trehalose (approximately 238 K for 50 wt% trehalose solution; Branca et al., 2001). Figure 5 shows the comparison of the TEM images for these three samples taken at the same magnification. Figure 5a verified that the TEM image obtained for the sample (a) was the same as that shown in Figure 1d. However, in samples (b) and (c), they found that most of the fine particles disappeared, and spherical or elongated flat surface areas were observed (Figures 5b and 5c). The edge of the flat surface area in the sample (c) has a slightly larger contrast than that in sample (b).

To determine the material of each phase observed in Figure 5, and to investigate the stability of ice Ic, the temperature ramping PXRD measurements were carried out every 10 K from 93 K to 273 K for the frozen samples of 47wt% trehalose concentration solution quenched in liquid nitrogen (Uchida & Takeya, 2010). The initial profile of the 47 wt% trehalose solution at 93K (the farthest side profile of Figure 6a) was similar to those in Figure 4, which was closed up in the 2θ range from 22° to 27°. Three large peaks with a high background indicated that this sample included both ice Ih and ice Ic crystals. The PXRD profile did not change during the temperature ramping experiment up to 233 K, but the profile drastically changed at 243 K; the three large diffraction peaks became sharpened and the base line decreased down to the noise level. These results indicate that the ice Ic phase disappeared between 233 and 243 K whereas the ice Ih still remained even above 243 K. At 273 K, the whole ice Ih signals disappeared due to its melting. Instead, the trehalose dihydrate crystal was formed simultaneously.

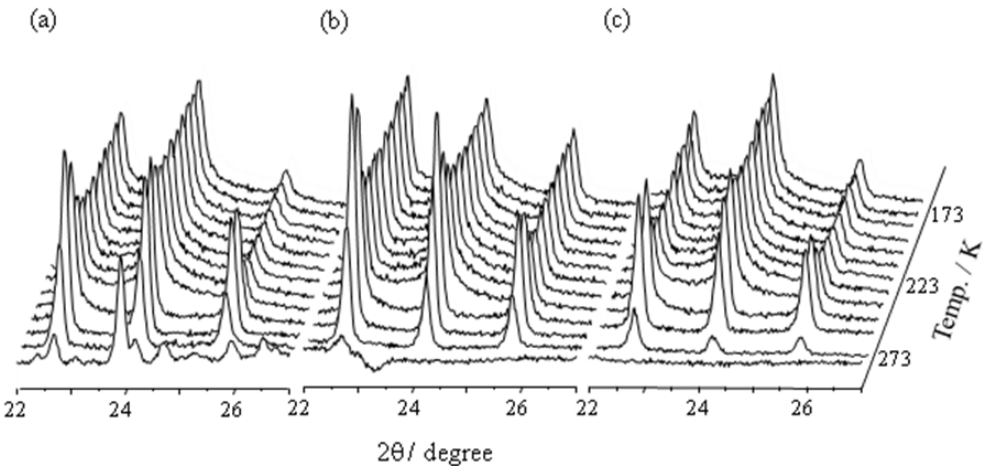

Fig. 6. Series of PXRD patterns of quenched samples of (a) 47 wt% concentrations of trehalose, (b) 50 wt% concentrations of sucrose, and (c) 47 wt% concentrations of maltose solutions with a temperature ramping from 93 K to 273 K in each 10 K. (Uchida & Takeya, 2010; reproduced by permission of the PCCP Owner Societies)

The temperature dependence of PXRD pattern was also observed in the 50 wt% sucrose (Figure 6b) and 47 wt% maltose (Figure 6c) solutions. The transition temperature from ice Ic to ice Ih in both samples was also observed between 233 and 243 K. These two samples showed, however, that no disaccharide crystal was formed at 273 K, that is, all solid phases

were melted at the ice melting point. These results suggest that trehalose forms its dihydrate crystal at temperatures above the ice melting point, whereas sucrose and maltose do not form their crystals at the same temperature.

As a conclusion, three typical features observed on the replica via TEM were identified by PXRD measurements; the smooth surface **S** as ice Ih crystallite, fine particles **P** having relatively uniform sizes ranging from 20 to 30 nm in diameter as disaccharide precipitation, and remaining part **R** as glassy material including ice Ic. Dependence of disaccharide concentrations on both ice Ih crystallite size and number concentration of fine particles suggested that disaccharide molecules inhibit the ice crystal growth with increasing in their concentrations.

Figure 6 also shows that ice Ic formed in the quenched disaccharide solutions is stable under anomalously higher temperatures. In a pure water system, ice Ic can be obtained by the following several methods: (1) from the high-pressure phase of ice (ice III or VII) by a decrease of pressure during an increase in temperature (Hobbs, 1974), (2) from the temperature increase of amorphous ice condensed on a cold surface (below 110 K) (Dewell & Rinfret, 1960), or (3) the quenching of a water droplet at a rate of 10^4 K s^{-1} (Bruggeller & Mayer, 1980; Dubochet & McDowall, 1981; Mayer & Hallbrucker, 1987; Johari, 2005). The ice Ic phase is metastable and it transforms to the stable ice Ih phase when it is warmed up above approximately 143 K and the reverse transformation is never observed.

However, the crystallographic observations of the frozen samples of the glycerol solution (Vigier et al., 1987; Berejnov et al., 2006), glucose solution (Kajiwara et al., 2008; Thanatuksora et al., 2008), and ionic salt solutions (Murray et al., 2005) have revealed that ice Ic was also formed in these quenching samples. Vigier et al. (1987) estimated the average diameter of ice Ic in the frozen glycerol solutions to be 5 to 15 nm. The ice Ic phase formed by quenching of the aqueous solutions mentioned above transformed to ice Ih above 200 K, which was obviously higher than that observed in the pure water system. This process is considered to occur naturally, that is, small droplets of water in the upper atmosphere may often freeze directly into ice Ic (Kobayashi et al., 1976; Whalley, 1981; Whalley, 1983; Takahashi & Kobayashi, 1983; Whalley & McLaurin, 1984). Mayer & Hallbrucker (1987) demonstrated that ice Ic formed in the quenched aqueous aerosol droplets and that it was stable up to approximately 200 K. Other studies had revealed that the ice Ic forms in confined space (Takamuku et al., 1997; Steytler et al., 1983; Christenson, 2001; Morishige & Iwasaki, 2003; Murray & Bertram, 2006). Takamuku et al. (1997) reported that ice Ic was formed from water existed in a porous silica of 3 nm and 10 nm in diameter. It was found that the ice Ic formed in the confined space was also stable at temperatures higher than that in the pure water system.

Taking into account these findings, the formation of ice Ic in disaccharide solutions is expected to occur in a confined meso-pore space formed during the quenching process. In general, the full-width of the half maximum intensity of the x-ray diffraction peaks expands (Jenkins & Snyder, 1996) when the crystallite size is several hundred nanometres or less. However, the diffraction peaks of ice Ih in the present study were not broadened even in the highest concentration sample. This suggest that the crystallite size of ice Ih would be ranged from micron to sub-micron order even if small fraction of amorphous ice appears in the presence of trehalose under condition of rapid quenching. Therefore, it is considered that the formation sites of ice Ih and ice Ic were different, and the crystallite size of ice Ih would be ranged from micron to sub-micron order. This is consistent with the results obtained by

the TEM image observations. Thus the ice Ic with less than a hundred nanometre in size was formed at the grain boundary between the ice Ih crystallites, and the disaccharide precipitated fine particles would provide the confined meso-pore space in the grain boundary.

The ice Ic would co-exist with the disaccharide precipitated particles, which may correspond to the giant disaccharide clusters (Gonda & Sei, 2005; Lerbret et al., 2005; Uchida et al., 2007; 2009). Moreover, the TEM images on the replica annealed at 150 K indicated that the fine particles disappeared whereas no profile changes in the PXRD were observed. If the ice Ic phase was formed on the fine particles, the ice Ic should be changed into the stable state at that moment. Thus we consider that the ice Ic would be formed between the disaccharide clusters by freezing of free water molecules, which locate around disaccharide molecules but are independent of the disaccharide clusters or glass phase.

The temperature ramping PXRD measurements on the rapid frozen sample of the highest concentration solutions indicated that the ice Ic phase was stable up to 233 K, which is much higher than that expected from the pure water system (approximately 143 K (Dewell & Rinfret, 1960)). This anomalous stability is similar to those reported in other solution systems (including glycerol (Vigier et al., 1987; Berejnov et al., 2006), glucose (Kajiwara et al., 2008; Thanatuksora et al., 2008), salts (Murray et al., 2005) or aqueous aerosol (Mayer & Hallbrucker, 1987)), or in the confined space systems (in porous silica (Takamuku et al., 1997) or in emulsion (Murray & Bertram, 2006)) as mentioned previously. Then the ice Ic phase is considered to be stabilized by foreign molecules. In the disaccharide solution system, the present study suggests that ice Ic exists between the disaccharide clusters. Then the water molecules constructing the ice Ic would slightly interact with disaccharide molecules even though they are not bound to the disaccharide molecules directly. The transition temperature from ice Ic to ice Ih was around 240 K which coincides well with the vitrification temperature (T_g') of the disaccharide solution; T_g' was approximately 238 K, 234 K and 233 K for the 50 wt% concentration of the trehalose, sucrose and maltose solutions, respectively (Branca et al., 2001). This is also the case for T_g'=230 K of glucose (Kajiwara et al., 2008; Thanatuksora et al., 2008) and for the eutectic point of 67 wt% glycerol at 230 K (Vigier et al., 1987; Berejnov et al., 2006). These coincidences allow us to consider that the transition of ice Ic to ice Ih is difficult to occur spontaneously in frozen solution systems because the foreign molecules might stabilize the system, but is induced by the high mobility of the foreign molecules. Therefore the transition of ice Ic to ice Ih observed in the present study may occur with the devitrification of the disaccharide molecules.

3. Inhibition process of ice crystal growth based on the viscosity measurement of disaccharide solutions via DLS measurement

To investigate the inhibition process of ice crystal growth by disaccharide molecules in the solution, we needed to know the dynamic properties of both water and disaccharide molecules. By comparison with the microscopic observations mentioned in the previous section, the macroscopic properties of the disaccharide solution, such as viscosity, would provide useful information. Uchida et al. (2009) measured the temperature and concentration dependence of viscosity of disaccharide solutions, especially for trehalose. They employed the dynamic light-scattering (DLS) spectroscopy method (Uchida et al., 2003) to measure the viscosity of aqueous solutions under wide-ranged conditions of temperature and concentration.

The brief explanations of the viscosity measurements are given here. Approximately 20 mm^3 of the solution was put in the sample cell for the DLS system. The temperature of the cell was controlled between 268 and 343 K with the accuracy of ±0.2 K by circulating silicone oil through a cooler. These temperatures are chosen to make the ratio between the glass-transition temperature T_g and the experimental temperature T, T_g/T, ranging from 0.4 to 0.6. The monochromatic light from an Ar-ion laser (20mW, λ=488 nm) was focused on the center of the sample cell. The light scattered by the uniform-sized latex particles in the solution was collected by an objective lens, and the time-dependent intensity of the mixing of scattered light through two pinholes was measured with the photomultiplier of the DLS spectrophotometer (Photal, DLS-7000). Since the Stokes–Einstein law was obeyed for the disaccharide solutions under the experimental conditions, the autocorrelation function $q_e(\tau)$ of the temporal fluctuations is computed by the photocurrent output and the translational diffusion coefficient of the solution D_τ from

$$q_e(\tau) = \exp(-D_\tau q^2 \tau) \tag{1}$$

where τ is the relative time and q is the scattering vector. The apparent particle diameter d, the viscosity η and the diffusion coefficient D_τ are related by the Stokes–Einstein law:

$$D_\tau = k_B T / A\, \eta d \tag{2}$$

where T is the absolute temperature, k_B is Boltzmann's constant, and A is a constant that depends on the type of friction between a material with d and its surrounding liquid (Corti et al., 2008). Substituting D_τ obtained by the DLS measurement and the latex particle size d = 204 nm, we obtained the viscosity of the solution around the small amount of light scattering materials (mass fraction of latex particles to be below 5×10^{-6}), which equals the absolute viscosity of the solution. Concerning the uncertainties of measurements and variation in the refractive indices, the uncertainty of viscosity measured by the DLS method was estimated to be ± 6%.

Figure 7 indicates η_{treha} (dots) with different trehalose concentrations C (wt%) measured at room temperature (300.3 ± 2.9 K). This figure indicates that η_{treha} increases with C. The data obtained by the DSL method was fitted by following equations (with a correlation of 0.99):

$$\eta_{treha} = 2.08\times10^{-4}C^3 - 8.68\times10^{-3}C^2 + 0.141C + 0.467 \tag{3}$$

which is shown in figure 7 as a dotted line. The cubic η–C relationship was proposed by Elias & Elias (1999). Recently, Longinotti & Corti (2008) summarized that the specific viscosity (η/η_w, where η_w is the viscosity of pure water at the same T (PROPATH, 1990)) related exponentially to molar concentration c (mol/kg). The obtained data were also checked by fitting the relation between η/η_w and c and the following fitting equation was obtained:

$$\ln(\eta_{treha}/\eta_w) = 0.900c - 0.0283 \tag{4}$$

with a correlation of 0.99 (data not shown). Equation (4) indicates the agreement of the data measured by the DLS method to the previous data. These results show that the relation between η and C is fitted by both models within the experimental conditions.

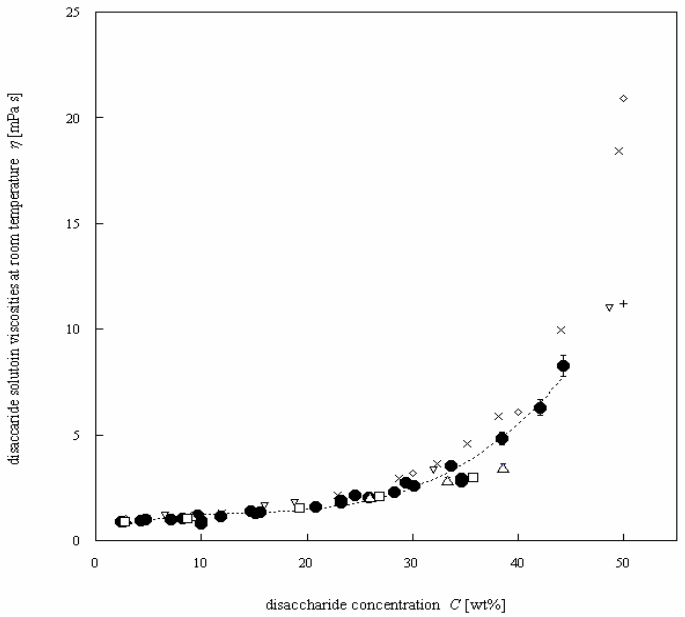

Fig. 7. Viscosities (η) of disaccharides vs. concentration (C) at room temperature. The dots indicate the relative viscosities of trehalose (η_{treha}), the open triangles indicate the relative viscosities of sucrose, and the open squares indicate the relative viscosities of maltose. The error bars for all the trehalose solution data indicate the maximum variations in η_{treha} observed in the DLS measurements, which are almost the same as the measurement uncertainties. The dotted line indicates the fitting curve for η_{treha} in Eq. (3). This figure also shows the η_{treha} near room temperature obtained by various conventional methods: open diamonds (Matsuoka et al., 2002), open inverted triangles (Magazù et al., 1999), ×-marks (Elias & Elias, 1999), and +-marks (Rampp et al., 2000). (Reprinted from Uchida et al., 2009, with permission from Elsevier.)

In addition, the data of η_{treha} were comparable with values in the literature for the bulk η_{treha} obtained by several conventional methods. In Figure 7, several reported viscosities measured using the conventional techniques are presented simultaneously. Most of the bulk viscosities of disaccharide solutions were measured by mechanical viscometers: the Ubbelohde viscometer (Magazù et al., 1999; Elieas & Elias, 1999; Branca et al., 2001), the Marion-Krieger Sisco capillary viscometer (Matsuoka et al., 2002), or the rotational viscometer (Nagasawa et al., 2003). The selected literature data plotted in Figure 7 were measured in a temperature range of 293.2–313.2 K.

Viscosities of other disaccharide solutions, sucrose (η_{suc}) and maltose (η_{mal}), were found to be similar to that of η_{treha} at a given concentration within the experimental uncertainties (shown in Figure 7). These three disaccharide solutions had very similar viscosity dependences of the viscosity-concentration relationships at room temperature, particularly in dilute solutions (less than 30 wt%).

On the other hand, the viscosity of a trehalose solution increases with decreasing temperature under all concentration conditions. Figure 8 depicts an Arrhenius plot of the

viscosity of trehalose solutions (all solid marks, + and ×). As a reference, the data for pure water is denoted with a thick dashed line. This figure also indicates that η_{treha} follows an Arrhenius temperature dependence ($\eta_{\mathrm{treha}} = \eta_0 \exp[Q_{\mathrm{treha}}/k_B T]$, where η_0 is constant and Q_{treha} is the temperature-dependence parameter for trehalose solution) under the experimental conditions. The temperature dependence fits the Arrhenius curve even below the melting point for solutions with any concentration. Therefore, below the melting point, the viscosity of a supercooled trehalose solution can be predicted by extrapolating the temperature dependence of the viscosity in the liquid state, at least within the experimental validity (i.e, the temperature is not below $T_g/0.6$ (Corti et al., 2008)).

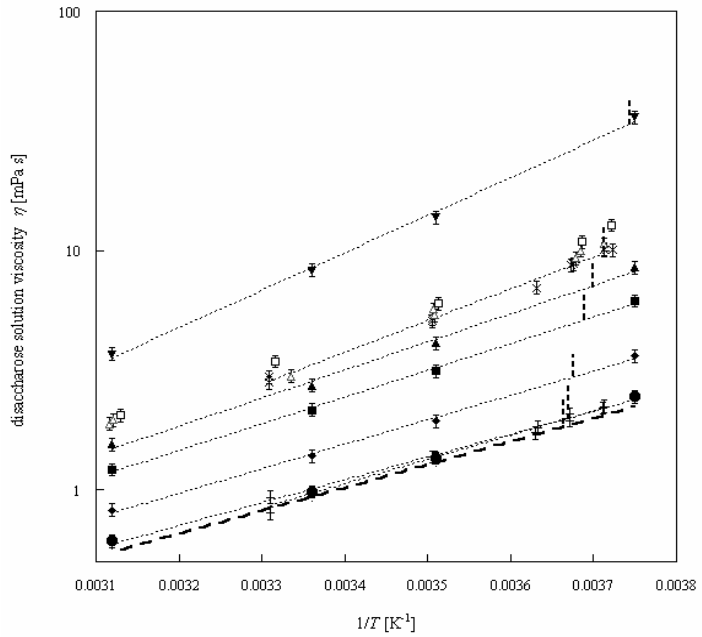

Fig. 8. Temperature dependence of viscosities for various concentrations of disaccharide solutions: η_{treha}, η_{suc}, and η_{mal}. Dots represent η_{treha} at a concentration of 4.75 wt%, crosses represent η_{treha} at a concentration of 9.93 wt%, solid diamonds represent η_{treha} at a concentration of 14.7 wt%, solid squares represent η_{treha} at a concentration of 24.5 wt%, solid triangles represent η_{treha} at a concentration of 29.4 wt%, ×-marks represent η_{treha} at a concentration of 34.7 wt%, and solid inverted-triangles, represent η_{treha} at a concentration of 44.3 wt%. The thin dotted line denotes the Arrhenius curve fit for each concentration. The thick dashed line indicates the temperature dependence of the viscosity of pure water, η_W (PROPATH, 1990). The thick short dotted vertical line on each curve is the melting point of the solution (Gonda & Sei, 2005). Open squares denote 38.5 wt% concentrations of sucrose solutions (η_{suc}), and triangles denote 35.8 wt% concentrations of maltose solutions (η_{mal}). (Reprinted from Uchida et al., 2009, with permission from Elsevier.)

The variation of the temperature-dependent parameter of trehalose solutions (Q_{treha}) with the solute concentration C indicates interesting properties: Q_{treha} for dilute solutions with

concentrations of less than 10 wt% is almost concentration-independent, which is the same as that of pure water (Q_w = 17.3 ± 1.4 kJ mol^{-1}). This indicates that the dynamic properties of dilute solutions are similar to those of pure water. This interesting result is very important when considering the cryoprotective effect of trehalose used in biological and engineering applications because trehalose is usually applied in dilute conditions of less than 10 wt%.

However, Q_{treha} increases linearly with an increase in C above 10 wt%. This result indicates that trehalose solutions have two types of structures in the liquid phase: a dilute solution (C<10 wt%) and a condensed solution (C>10 wt%). Since the values of Q_{treha} in the condensed solutions increased linearly with C, the macroscopic properties of solutions were assumed to be continuously changing with trehalose concentration.

In the dilute trehalose solutions, the major matrix of the solutions is pure water (or free water) and the trehalose molecules exist as minor solute materials. Since the viscosity in these solutions is nearly the same as pure water viscosity, it is concluded that the trehalose molecules make only a small contribution to the macroscopic solution properties, or to the hydrogen-bonding network of the free-water molecules, even though the trehalose molecules tend to break the hydrogen-bond network of water (Branca et al., 1999a; Branca et al., 1999b; Branca et al., 1999c; Magazù et al., 2004; Nagasawa et al., 2003).

In the condensed trehalose solutions, most of free-water molecules are bound to trehalose molecules because of their high hydration abilities (the hydration number of trehalose is estimated to be 11 ± 4 (Lerbret et al., 2005)). The dynamic structure of the solution is then changed from a hydrogen-bond network of free water to a network structure related to hydrated-trehalose molecules with increasing in the trehalose concentration, which contributes to the viscosity of the solution. Thus, Uchida et al. (2009) employed the parameter W as the free-water ratio of the solution, W = (free water)/(total water), to consider the change in the network structure of the solution by the following equation:

$$W = (1 - C/C_s)/(1 - C/100) \tag{5}$$

where C_s is the saturation concentration of the trehalose solution. Based on the trehalose hydration number mentioned above, C_s is estimated to be 63 ± 7 wt%. Using this equation, the dilute condition corresponds to W exceeding approximately 93%.

As expected, Q_{treha} increases linearly with a decrease in W for W < 90% (Figure 9). Since Q_{treha} is an energy term, the increase in Q_{treha} for the condensed solutions is a reflection of the higher energy barriers in the translational motion of bound molecules, or an increase in the activation energy of the self-diffusion coefficients of both water and trehalose molecules. The self-diffusion coefficients of either solute or solution molecules in disaccharide solutions were previously measured by NMR spectroscopy (Ekdawi-Sever et al., 2003; Rampp et al., 2000). From these reported values, the activation energies for both molecules were found to increase gradually with a decrease in W. Therefore, the energy barrier for the translational motion of the matrix is caused mainly by the lack of free water.

A solute–solution model of low-W (or high-C) solutions has been proposed by molecular dynamics (MD) simulation (Lerbret et al., 2005). The simulation study suggested that the hydrated clusters of disaccharide molecules began to interact, forming compartment-like hydrogen-bonding networks. These clusters were consistent with the giant hydrated-saccharide clusters (Gonda & Sei, 2005; Lerbret et al., 2005), which also corresponded to the fine particles found in TEM images (Uchida et al., 2007). Therefore, a network structure with a high-energy barrier for the translational motion of the matrix was assumed to be built with

these giant hydrated disaccharide clusters. Since Q_{treha} changes continuously, the phase change of the network structure from a free-water matrix to a disaccharide cluster matrix would progress partially in the solution.

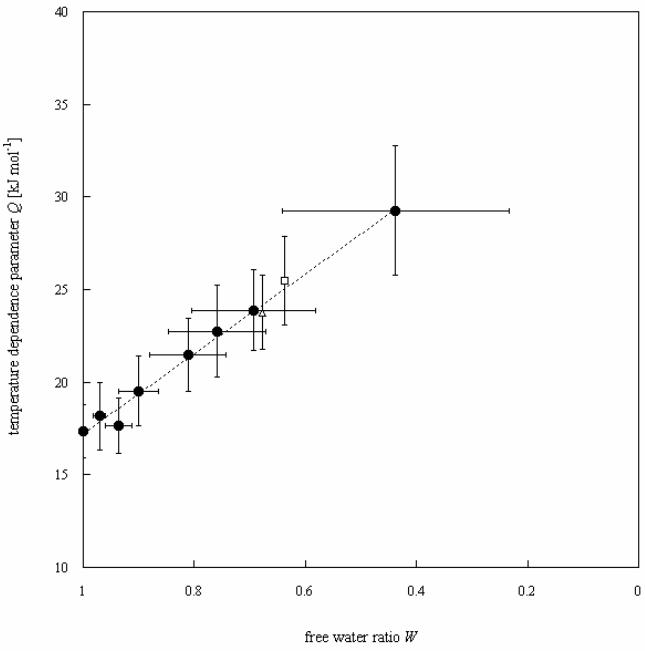

Fig. 9. Temperature dependence parameter of trehalose solutions (Q_{treha}) (dots) vs. the free-water ratio (W) estimated by Eq. (5). The Q_{suc} estimated from the experimental data presented in Fig. 8 is denoted by open squares, and Q_{mal} estimated from the experimental data presented in Fig. 8 is denoted by open triangles. Error bars for the W estimation were caused by the uncertainty of the hydration number (Lerbret et al., 2005), and those for Q were from the standard deviations of the Q estimate in Fig. 8. (Reprinted from Uchida et al., 2009, with permission from Elsevier.)

4. Frozen mechanism of trehalose solution and its cryopreservation effect for living cells

Above the melting point, the volume ratio of free water W decreases with an increase in C. The remaining region is the trehalose-binding (or hydrated) water which forms trehalose-rich clusters and the clusters tend to bind each other to construct the macroscopic cluster-binding network in high C solutions. We assumed that this network would correspond to a compartment-like structure in the solution (Lerbret et al., 2005), which gradually develops with an increase in C. Since this network develops all over the solution, its bulk viscosity increases.

When a small amount of solution was quenched at the liquid nitrogen temperature, the disaccharide molecules forming the giant clusters would construct the fine particles observed

in the TEM images. On the other hand, the free water molecules free from the disaccharide molecules form ice Ih crystallites. The crystallite size of the ice Ih is larger than the sub-micron order. Then ice Ih crystallite is determined as the smooth surface area in the TEM images. The intermediate region of these phases is constructed by water molecules which are located in the compartment-like structure comprised by the giant clusters. These water molecules form the metastable ice Ic crystal because the compartment-like structure is considered to be the meso-pore space stabilizing ice Ic (Fig. 10). When the disaccharide concentration is high, a large amount of the compartment-like structures would be formed between the giant clusters. Then the total amount of ice Ic was larger in higher disaccharide concentration samples. In addition, the compartment-like structure would divide the space for free water, a number of nucleation sites of ice Ih also increases although the volume of free-water used for the ice Ih formation decreases. Thus the crystal growth of ice Ih is inhibited in the higher-concentration disaccharide solutions. Since these ice Ic crystals were anomalously stable up to 233 K, the compartment-like structure would be maintained until the disaccharide molecules change their molecular network at their vitrification temperatures.

On the other hand, when the trehalose solution is frozen slowly, the dihydrate trehalose crystal is formed prior to ice formation. At that moment, approximately 80% of water molecules bounded to a trehalose molecule is released. Thus the formation of dihydrated trehalose crystal increases the ratio of free water *W* and reduces the cluster-binding network in the solution. Therefore, the slow freezing process would lose the effect of cryopreservation effect of trehalose.

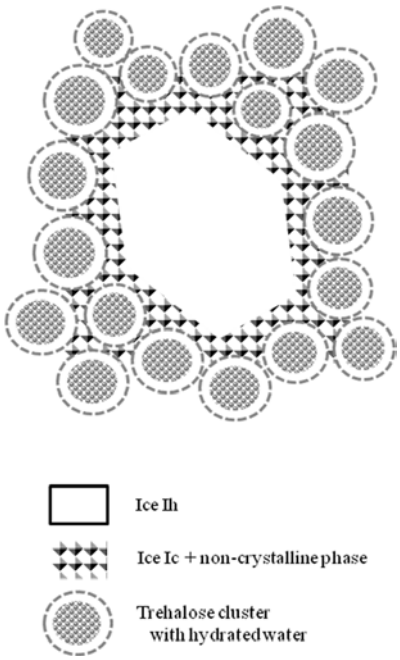

Fig. 10. Phase separation image during the freezing of the disaccharide solutions. (Uchida & Takeya, 2010; reproduced by permission of the PCCP Owner Societies)

Since the size of disaccharide molecules are too large to permeate the biomembrane, they cannot contribute to the inhibition of the intracellular freezing by reducing the melting point due to the molar freezing point depression effect. Thus the cryopreservation mechanism of disaccharide is different from the cell-permeable cryoprotectants, such as glycerol or of DMSO. Some cryopreservation tests for the primary cells having weak tolerance for cryopreservations demonstrate the difference between these cyroprotectants. Motomura et al. (2007) reported the provability of cryopreservation of the primary cells of neonatal rat cortical neurons with 10% DMSO but not with trehalose. Later, we carried out further experiments and verified the viability of the neurons related to the concentrations of DMSO (solid circles) and trehalose (open squares) at wider range (Fig. 11). On the other hand, Miyamura et al. (2010) reported the viability of cryopreserved neonatal rat cardiac myocytes depending on the DMSO concentration. We expanded their researches to the cryopreservation with trehalose. Figure 12 shows the viability of cryopreserved cardiac myocytes depending on the DMSO (solid circles) and trehalose (open squares) concentration. Figures 11 and 12 indicate that both neurons and cardiac myocytes can be cryopreserved with DMSO, which has the optimum concentration at approximately 10%. However, both primary cells cannot be cryopreserved by trehalose at any concentrations under their experimental conditions. Since these cryopreservation tests were carried out by relatively slow freezing process (approximately –10 K min^{-1} in the cooling rate), it is considered that trehalose cannot act as the effective cryoprotectant at those cooling rates. This is consistent with the prediction of the slow freezing process of disaccharide solutions mentioned previously. Concerning the fact that the cryoprotectant DMSO loses its cryoprotective effect when the neuron was quenched in liquid nitrogen (Uchida et al., 2007), it is considered that cryoprotectants have optimized cooling rates in addition to concentrations which relate to the frozen mechanism of the solution.

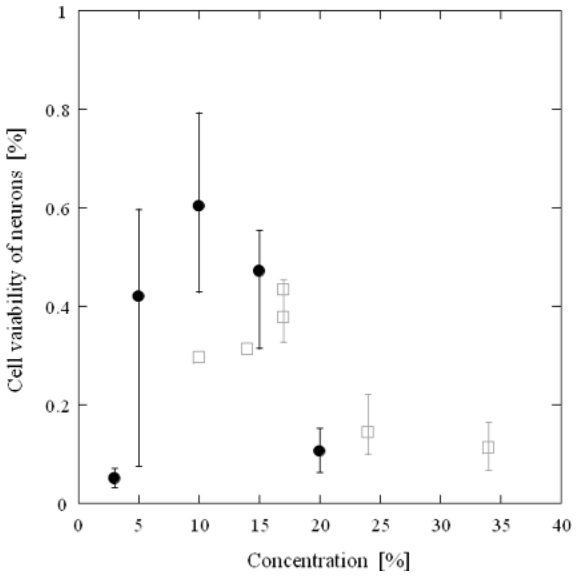

Fig. 11. Cell viability of rat cortical neurons cryopreserved by DMSO (solid circles) and trehalose (open squares) at various concentrations.

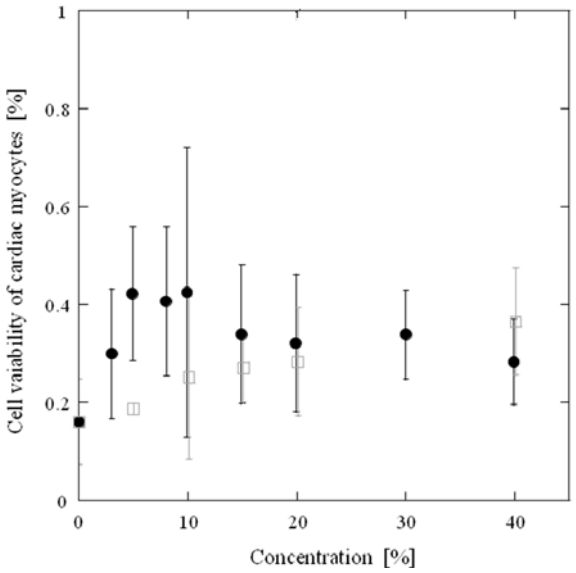

Fig. 12. Cell viability of rat cardiac myocytes cryopreserved by DMSO (solid circles) and trehalose (open squares) at various concentrations. (DMSO data are modified after Miyamura et al., 2010)

Therefore, we conclude that the cell-permeable cryoprotectants act well in the slow freezing process whereas the cell-impermeable cryoprotectants are feasible in the quench process. Since DMSO, as cell-permeable cryoprotectants, reduces the melting point of cytosol to protect the intracellular freezing, they require the habituation time to penetrate into cytosol. On the other hand, trehalose, as a cell-impermeable cryoprotectant, cannot act well in the slow freezing process since it crystallizes at temperatures above the melting point. Thus the optimization of trehalose would be revealed in the quenching process. At that condition, the formation of ice Ic would be a useful marker showing the growth inhibition of ice Ih crystallites.

5. Conclusion

Disaccharides are expected to be the natural cryoprotective agents for living bodies and cells. However, since they are too large to permeate the biomembrane, the cryopreservation mechanism has not been revealed. This review shows several experimental approaches to investigation of the freezing process of disaccharide solutions, especially trehalose solution.
The combination of the transmission electron microscopic observations of freeze-fractured replica films with the powder x-ray diffraction (PXRD) measurements of the quenched trehalose solutions revealed that the crystal growth of ice Ih crystallites in the quenched sample is inhibited by the formation of the giant hydrated-trehalose clusters which construct the compartment-like structures binding with each other. This is confirmed by the formation and anomalous stability of ice Ic. The stability of ice Ic is extended as high as approximately 243 K because the meso-pore space stabilizing ice Ic is maintained until the trehalose molecules change their hydrogen-bonded network at the vitrification temperature. This

condensed phase is confirmed to exist in liquid phase above the melting point by measuring the viscosity of the bulk liquid with dynamic light scattering method and by PXRD measurements with temperature ramping. However, when the trehalose solution is cooled slowly, the dihydrate trehalose crystal is formed prior to the ice formation. Thus trehalose would lose the cryopreservation effect in the slow freezing method.
Therefore, the disaccharide molecules are considered to act as the cell-impermeable cryoprotectants when the cell-dispersed solution is rapidly frozen. These predictions are qualitatively verified by several cryopreservation tests for the primary cells having weak tolerance for cryopreservation, such as the rat cortical neurons and rat cardiac myocytes.

6. Acknowledgment

Trehalose and maltose were donated by Hayashibara Biochemical Labs., Inc. The freeze-fracture replica observations by TEM were technically supported by Mr. A. Okutomi (JEOL), Dr. Shibayama, and Dr. N. Sakaguchi (Hokkaido Univ.). The DLS measurements were technically supported by Dr. H. Kaga (AIST). The cryopreservation experiments were carried out by Mr. J. Motomura and Mr. K. Miyamura (Hokkaido Univ.). Authors acknowledge for the reuse permission of the published artworks to Elsevier and the Royal Society of Chemistry. Part of this work was supported financially by the Grant-in-Aid for Scientific Research from the Japan Society for the Promotion of Science.

7. References

Akao, K., Okubo, Y., Masago, H., Asakawa, N., Inoue, Y., Sakurai, M. (2001). FTIR study of the properties of anhydrous form II of trehalose (in Japanese with English abstract). *Cryobio. Cryotech.*, Vol. 47, pp. 23–26

Berejnov, V., Husseini, N. S., Alsaied, O. A., Thorne, R. E. (2006). Effects of cryoprotectant concentration and cooling rate on vitrification of aqueous solutions. *J. Appl. Cryst.*, Vol. 39, pp. 244-251

Branca, C., Magazù, S., Maisano, G., Migliardo, P. (1999a). Anomalous cryoprotective effectiveness of trehalose: Raman scattering evidences. *J. Chem. Phys.*, Vol. 111, pp. 281–287

Branca, C., Magazù, S., Maisano, G., Migliardo, P., Villari, V., Sokolov, A. P. (1999b). The fragile character and structure-breaker role of α,α−trehalose: viscosity and Raman scattering findings. *J. Phys.: Condense. Matter*, Vol. 11, pp. 3823-3832

Branca, C., Magazù, S., Maisano, G., Migliardo, P. (1999c). α,α−Trehalose -water solutions. 3. Vibrational dynamics studies by inelastic light scattering. *J. Phys. Chem. B*, Vol. 103, pp. 1347-1353

Branca, C., Magazù, S., Maisano, G., Migliardo, P., Migliardo, F., Romeo, G. (2001). α,α−Trehalose/water solutions. 5. Hydration and viscosity in dilute and semidilute disaccharide solutions. *J. Phys. Chem. B*, Vol. 105, pp. 10140-10145

Bruggeller, P., Mayer, E. (1980). Complete vitrification in pure liquid water and dilute aqueous-solutions. *Nature*, Vol. 288, pp. 569-571

Christenson, H. K. (2001). Confinement effects on freezing and melting. *J. Phys.: Condens. Matter*, Vol. 13, No. 11, R95-R133

Corti, H. R., Frank, G. A., Marconi, M. C. (2008). Diffusion-viscosity decoupling in supercooled aqueous trehalose solutions. *J. Phys. Chem. B*, Vol. 112, pp. 12899-12906

Crowe, J. H., Crowe, L. M., Carpenter, J. F., Rudolph, A. S., Wistrom, C. A., Spargo, B. J., Anchrodoguy, T. J. (1988). Interactions of sugars with membranes. *Biochim. Biophys. Acta.*, Vol. 947, pp. 367–384

Dewell, L. G., Rinfret, A. P. (1960). Low-temperature forms of ice as studied by x-ray diffraction. *Nature*, Vol. 188, pp. 1144-1148

Dubochet, J., McDowall, A. W. (1981). Vitrification of pure water for electron-microscopy. *J. Microsc.*, Vol. 124, RP3-RP4

Ekdawi-Sever, N., de Pablo, J. J., Feick, E., von Meerwall, E. (2003). Diffusion of sucrose and α,α–Trehalose in aqueous solutions. *J. Phys. Chem. A.*, Vol. 107, pp. 936-943

Elieas, M. E., Elias, A. M. (1999). Trehalose+water fragile system: properties and glass transition. *J. Molecular Liquids*, Vol. 83, pp. 303-310

Gonda, T., Sei, K. (2005). The inhibitory growth mechanism of saccharides on the growth of ice crystals from aqueous solutions. *Progress in Crystal Growth and Characterization of Materials,* Vol. 51, pp. 70-80

Hobbs, P. V. (1974). *Ice Physics*, Clarendon. Oxford, Oxford

Jenkins, R., Snyder, R. L. (1996). Introduction to X-ray powder diffractometry. *Chemical analysis* (ed. Winefordner J. D.), John Wiley & Sons, Inc., New York, pp. 89-91

Johari, G. P. (2005). Water's size-dependent freezing to cubic ice. *J. Chem. Phys.*, Vol. 122, pp. 194504-1-5

Kajiwara, K., Thanatuksom, P., Murase, N., Franks, F. (2008). Cubic ice can be formed directly in the water phase of vitrified aqueous solutions. *CryoLett.*, Vol. 29, No. 1, 29-34

Kanno, H., Yamazaki, Y. (2001). Raman study of aqueous solutions of disaccharides including trehalose (in Japanese with English abstract). *Cryobio. Cryotech.*, Vol. 47, pp. 76–79

Kobayashi, T., Furukawa, Y., Takahashi, T., Uyeda, H. (1976). Cubic structure models at the junctions inpolycrystalline snow crystals. *J. Cryst. Growth*, Vol. 35, pp. 262-268

Kuhs, W. F., Bliss, D. V., Finney, J. L. (1987). High-resolution neutron powder diffraction study of ice Ic. *J. Physique*, Vol. 48, No. C-1, 631-636

Lerbret, A., Bordat, P., Affouard, F., Descamps, M., Migliardo, F. (2005). How homogeneous are the trehalose, maltose, and sucrose water solutions? An insight from molecular dynamics simulations. *J. Phys. Chem. B*, Vol. 109, pp. 11046-11057

Longinotti, M. P., Corti, H. R. (2008). Viscosity of concentrated sucrose and trehalose aqueous solutions including the supercooled regime. *J. Phys. Chem. Ref. Data*, Vol. 37, No. 3, pp. 1503-1515

Magazù, S., Maisano, G., Migliardo, P., Tettamanti, E., Villari, V. (1999). Transport phenomena and anomalous glass-forming behaviour in α,α−trehalose aqueous solutions. *Molecular Physics,* Vol. 96, No. 3, pp. 381-387

Magazù, S., Maisano, G., Migliardo, P., Mondelli, C. (2004). α,α–trehalose /water solutions. VII: an elastic inhoherent neutron scattering study on fragility. *J. Phys. Chem. B*, Vol. 108, pp. 13580-13585

Matsuoka, T., Okada, T., Murai, K., Koda, S., Nomura, H. (2002). Dynamics and hydration of trehalose and maltose in concentrated solutions. *J. Molecular Liquids*, Vol. 98–99, pp. 317-327

Mayer, E., Hallbrucker, A. (1987). Cubic ice from liquid water. *Nature*, Vol. 325, pp. 601-602

Miyamura, K., Nagayama, M., Gohara, K., Taira, T., Shimizu, K., Sakai, M., Uchida, T. (2010). Evaluation of viability of cryopreserved rat cardiac myocytes and effects of dimethyl sulfoxide concentration on cryopreservation (in Japanese with English abstract). *Cryobio. Cryotech.*, Vol. 56, No. 2, pp. 111–117

Morishige, K., Iwasaki, H. (2003). X-ray study of freezing and melting of water confined within SBA-15. *Langmuir*, Vol. 19, No. 7, pp. 2808-2811

Motomura, J., Uchida, T., Nagayama, M., Gohara, K., Taira, T., Shimizu, K., Sakai, M. (2007). Effects of additives and cooling rates on cryo-preservation process of rat cortical cells. *Physics and Chemistry of Ice* (Ed. Kuhs, W. F.), Royal Society of Chemistry, London, pp. 409-416

Murray, B. J., Knopf, D. A., Bertram, A. K. (2005). The formation of cubic ice under conditions relevant to Earth's atmosphere. *Nature*, Vol. 434, pp. 202-205

Murray, B. J., Bertram, A. K. (2006). Formation and stability of cubic ice in water droplets. *Phys. Chem. Chem. Phys.*, Vol. 8, pp. 186-192

Nagasawa, Y., Nakagawa, Y., Kenmochi, J., Okada, T. (2003). Microscopic viscosity of aqueous solution of saccharides: A study by ultrafast pump-probe spectroscopy. *Cryobio. Cryotech.*, Vo. 49, No. 2, pp. 87-95

PROPATH - a Program Package for Thermophysical Properties of Fluids, Ver. 7.1. (1990). Corona Publishing, Tokyo

Rampp, M., Buttersack, C., Lüdemann, H. –D. (2000). c, T-dependence of the viscosity and the self-diffusion coefficients in some aqueous carbohydrate solutions. *Carbohyd. Res.*, Vol. 328, pp. 561-572

Sei, K., Gonda, T., Arima, Y. (2001). Freezing of the solution of trehalose and water (in Japanese with English abstract). *Cryobio. Cryotech.*, Vol. 47, pp. 9–12

Sei, K., Gonda, T., Arima, Y. (2002). Growth rate and morphology of ice crystals growing in a solution of trehalose and water. *J. Crystal Growth*, Vol. 240, pp. 218–229

Sei, K., Gonda, T. (2004). Melting points of ice crystals growing in sugar solutions (in Japanese with English abstract). *Cryobio. Cryotech.*, Vol. 50, pp. 93–95

Steytler, D. C., Dore, J. C., Wright, C. J. (1983). Neutron-diffraction study of cubic ice nucleation in a porous silica network. *J. Phys. Chem.*, Vol. 87, No. 14, pp. 2458-2459

Sum, A. K., Faller, R., de Pablo, J. J. (2003). Molecular simulation study of phospholipids bilayers and insights of the interactions with disaccharides. *Biophys. J.* Vol. 85, pp. 2830–2844

Takahashi, T., Kobayashi, T. (1983). The role of the cubic structure in freezing of a supercooled water droplet on an ice substrate. *J. Cryst. Growth*, Vol. 64, pp. 593-603

Takamuku, T., Yamagami, M., Wakita, H., Masuda, Y., Yamaguchi, T. (1997). Thermal property, structure, and dynamics of superlooled water in porous silica by calorimetry, neutron diffraction, and NMR relaxation. *J. Phys. Chem. B*, Vol. 101, pp. 5730-5739

Thanatuksora, P., Kajiwara, K., Murase, N., Franks, F. (2008). Freeze-thaw behaviour of aqueous glucose solutions – the crystallisation of cubic ice. *Phys. Chem. Chem. Phys.*, Vol. 10, pp. 5452-5458

Uchida, T., Ohmura, R., Nagao, J., Takeya, S., Ebinuma, T., Narita, H. (2003). Viscosity of aqueous CO_2 solutions measured by dynamic light scattering. *J. Chem. Eng. Data*, Vol. 48, No. 5, 1225-1229

Uchida, T., Nagayama, M., Shibayama, T., Gohara, K. (2007). Morphological investigations of disaccharide molecules for growth inhibition of ice crystals. *J. Crystal Growth*, Vol. 299, No. 1, pp. 125-135

Uchida, T., Nagayama, M., Gohara, K. (2009). Inhibition process of ice crystal growth in trehalose solutions: Interpretation by viscosity measurements using dynamic light scattering method. *J. Crystal Growth*, Vol. 311, No. 23-24, pp. 4747-4752

Uchida, T., Takeya, S. (2010). Powder X-ray diffraction observations of ice crystals formed from disaccharide solutions. *Phys. Chem. Chem. Phys.*, Vol. 12, No. 45, pp. 15034-15039

Vigier, G., Thollet, G., Vassoille, R. (1987). Cubic and hexagonal ice formation in water-glycerol mixture (50% w/w). *J. Cryst. Growth*, Vol. 84, pp. 309-315

Wang, Y., Tominaga, Y. (1994). Dynamical structure of water in aqueous solutions of D-glucose and D-galactose by low-frequency Raman scattering. *J. Chem. Phys.* Vol. 100, pp. 2407–2412

Whalley, E. (1981). Scheiners halo – evidence for ice Ic in the atmosphere. *Science*, Vol. 211, 389-390

Whalley, E. (1983). Cubic ice in nature. *J. Phys. Chem.*, Vol. 87, No. 21, pp. 4174-4179

Whalley, E., McLaurin, G. E. (1984). Reraction halos in the solar-system 1. Halos from cubic-crystals that may occur in atmospheres in the solar-system. *J. Opt Soc. Am.*, Vol. A1, No. 12, pp. 1166-1170

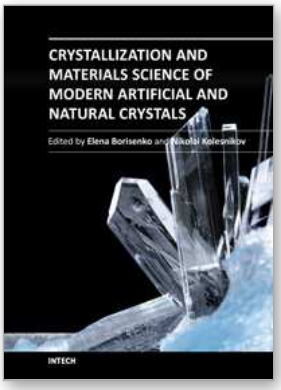

Crystallization and Materials Science of Modern Artificial and Natural Crystals

Edited by Dr. Elena Borisenko

ISBN 978-953-307-608-9
Hard cover, 328 pages
Publisher InTech
Published online 20, January, 2012
Published in print edition January, 2012

Crystal growth is an important process, which forms the basis for a wide variety of natural phenomena and engineering developments. This book provides a unique opportunity for a reader to gain knowledge about various aspects of crystal growth from advanced inorganic materials to inorganic/organic composites, it unravels some problems of molecular crystallizations and shows advances in growth of pharmaceutical crystals, it tells about biomineralization of mollusks and cryoprotection of living cells, it gives a chance to learn about statistics of chiral asymmetry in crystal structure.

InTech Europe
University Campus STeP Ri
Slavka Krautzeka 83/A
51000 Rijeka, Croatia
Phone: +385 (51) 770 447
Fax: +385 (51) 686 166
www.intechopen.com

InTech China
Unit 405, Office Block, Hotel Equatorial Shanghai
No.65, Yan An Road (West), Shanghai, 200040, China
中国上海市延安西路65号上海国际贵都大饭店办公楼405单元
Phone: +86-21-62489820
Fax: +86-21-62489821